

E-VLC: A Real-World Dataset for Event-based Visible Light Communication And Localization

Shintaro Shiba Quan Kong Norimasa Kobori
Woven by Toyota

Abstract

Optical communication using modulated LEDs (e.g., visible light communication) is an emerging application for event cameras, thanks to their high spatio-temporal resolutions. Event cameras can be used simply to decode the LED signals and also to localize the camera relative to the LED marker positions. However, there is no public dataset to benchmark the decoding and localization in various real-world settings. We present, to the best of our knowledge, the first public dataset that consists of an event camera, a frame camera, and ground-truth poses that are precisely synchronized with hardware triggers. It provides various camera motions with various sensitivities in different scene brightness settings, both indoor and outdoor. Furthermore, we propose a novel method of localization that leverages the Contrast Maximization framework for motion estimation and compensation. The detailed analysis and experimental results demonstrate the advantages of LED-based localization with events over the conventional AR-marker-based one with frames, as well as the efficacy of the proposed method in localization. We hope that the proposed dataset serves as a future benchmark for both motion-related classical computer vision tasks and LED marker decoding tasks simultaneously, paving the way to broadening applications of event cameras on mobile devices. <https://woven-visionai.github.io/evlc-dataset>

1. Introduction

Optical communication from infrastructure to cameras, such as QR code and AR markers, has a wide range of applications from mobile payment to localization in our daily lives. These QR and AR markers are recognized mainly using conventional frame-based cameras, however, recently active markers that modulate visible light (e.g., LED) at high frequencies have gained attention thanks to event cameras that offer high spatio-temporal resolution. However, due to the novelty of the camera, there have been no public datasets or detailed analyses for such visible light communication (VLC). Furthermore, it poses unique challenges for

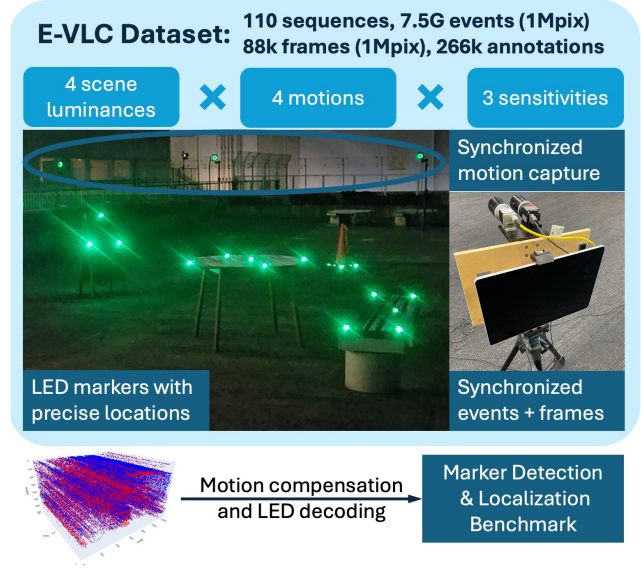


Figure 1. We propose the E-VLC dataset and a novel method that compensates motion to improve the localization accuracy. The dataset consists of synchronized events, frames, and GT poses as well as bounding boxes, in various recording settings.

typical event-based vision methods to simultaneously process the high-frequency LED and motion data, since the LEDs break the commonly-used brightness constancy assumption. Prior work have shown that event cameras in VLC can be used both for receiving information and localization of moving markers (i.e., with a static camera) or a moving camera (i.e., with static markers). However, the evaluation is challenging, especially where the camera moves, since it requires the ground truth (GT) poses.

In this work, we present *E-VLC*, the first event camera dataset that consists of events and frames at high resolution (1-Mpixel) with ground-truth poses from motion capture, all of which are calibrated and accurately synchronized (Fig. 1). Precise synchronization is achieved by using an external trigger box that sends hardware triggers to the motion capture and the cameras on the mobile (hand-held) recording system. The dataset offers various recording scenarios, including (i) different types of motion (static, rotation,

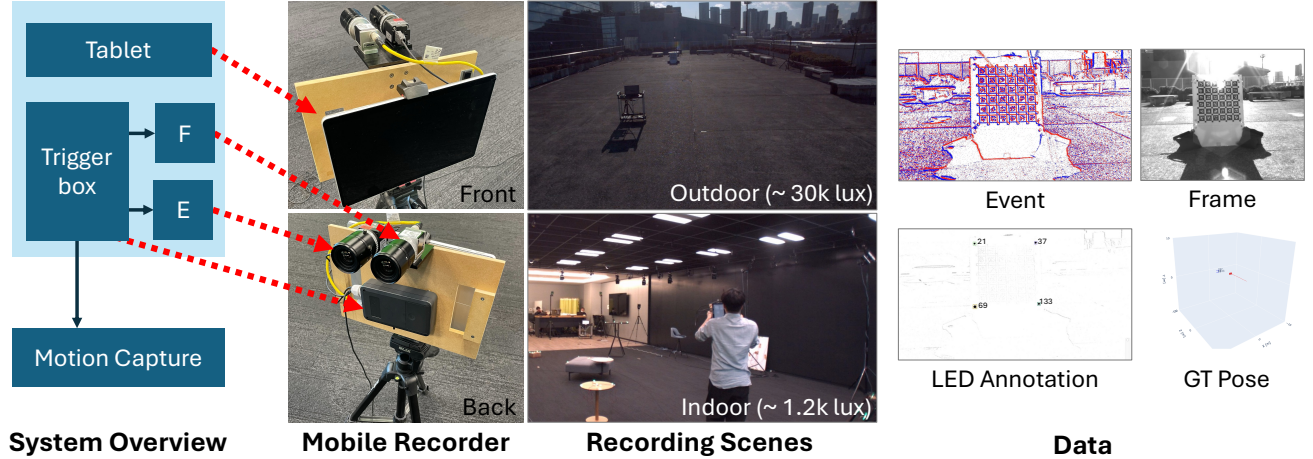


Figure 2. Data recording setup. The mobile recorder consists of two cameras (1280×1024 -pix frame and 1280×720 -pix event) that are synchronized via a trigger box and a tablet. The trigger sends the signal to the external motion capture. We record the data both in outdoor and indoor environments for different scene luminance. Best viewed online.

Table 1. Comparison of different sensors for VLC.

	Temporal resolution	Spatial resolution
Photodiode	High (M–GHz)	Low
Frame camera	Low (< 100 Hz)	High
Event camera	High (< 1 MHz)	High

translation, and dynamic), (ii) various scene luminance in both indoor and outdoor settings, and (iii) different event camera sensitivities. We also publish annotations of LED bounding boxes.

Detecting and decoding modulated LED signals from a moving event camera is challenging, since such scenes include event data from moving edges and flickering LEDs. Furthermore, due to the pixel displacements of the detected LEDs, the localization accuracy may deteriorate. To this end, we propose a novel method that combines motion estimation and compensation for localization. The experimental results show that (i) despite the lack of brightness constancy, the Contrast Maximization framework helps estimate motion in such scenarios and (ii) the proposed motion compensation improves localization.

In summary, this work presents several distinctive contributions in event-based optical communication:

1. The first public dataset for VLC applications using event cameras. The dataset consists of precisely synchronized events, frames, ground-truth pose of LED markers and cameras, and bounding-box annotations for LEDs. It also includes various recording conditions (motion type, scene luminance, event camera sensitivity) to cover real-world applications.
2. Detailed analysis of the data under different settings, such as effective distance and comparison with frame-

based methods. It helps the holistic understanding of the dataset that includes flickering LEDs and scene motion.

3. A novel LED-based localization method that leverages motion compensation with Contrast Maximization. The experimental results show the proposed method successfully compensates motion and improves LED detection and localization.

With these contributions, this work will serve as a future benchmark for LED detection and LED-based localization tasks using event cameras. We hope that the dataset under various practical scenarios will accelerate event camera applications, especially on edge devices such as AR glasses and mobiles, broadening the community [33].

2. Related Work

Visible light communication (VLC) that utilizes modulated LEDs at high frequencies has been known since the early 2000s [39]. Compared with wireless communication using radio frequency (RF), VLC offers advantages such as high reliability and secure connections. However, the lack of suitable receivers prevents VLC from wide adaptation (Tab. 1). Conventional frame-based cameras (CMOS/CCD) are not suitable for large data bandwidth, because their temporal resolution (typically 10–100 Hz) is limited [23, 40]. Photodiodes offer a high temporal resolution (typically on the order of GHz), while they do not have enough spatial resolution that is necessary for separating different sources and localization [3]. Optical communication using event cameras has recently been an emerging topic in event-based vision research. Event cameras achieve a high temporal resolution (typically up to 1–10 μ s) and a high spatial resolution (up to 1 Mpix), making them an ideal receiver, as shown in Tab. 1. Also, they offer other advantages such as high dy-

Table 2. Dataset summary.

Motion	Luminance [lx]	Sensitivity	Sequences	Duration [s]	Events	Frames	Annotations
Static	600, 1200, 30k	Low	27	128.5	22M	2976	8928
		Medium	23	71.7	82M	960	2880
		High	23	107.8	225M	2148	6444
Translation	600, 1200	Low	6	378.4	41M	13629	40861
		Medium	4	242.7	1129M	8005	23997
		High	2	90.2	767M	3097	9284
Rotation	600, 1200	Low	4	168.9	25M	6376	19128
		Medium	4	208.7	1135M	6991	20973
		High	4	252.0	2031M	9092	27276
Dynamic	10, 600, 1200	Low	5	356.1	62M	13400	40171
		Medium	5	386.0	983M	13954	41841
		High	3	221.0	978M	8139	24404
Total	10, 600, 1200, 30k	L, M, H	110	2612.0	7.5G	88.7k	266.2k

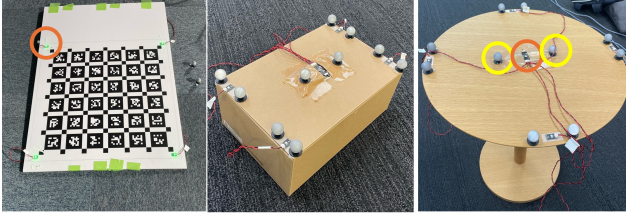


Figure 3. LED markers on different objects. Orange circles indicate the LEDs, each of which transmits different ID signals. Yellow circles are markers for the motion capture system.

dynamic range, since they output only differences of logarithmic intensities [20, 24], making them serve as “eyes” for robots (e.g., mobile, automotive, drones) [13].

Previous work have shown various VLC applications with event cameras on different modulation protocols. Protocols can be categorized into four: blink-based, frequency-based, interval-based, and change-based. The blink-based protocol encodes the binary information as the binary ON/OFF of the illumination, i.e., blink. Preliminary work analyzes different transmission rates (bps) at different distances in static scenes [38]. Localization under static environments is also tested in [18]. The frequency-based protocol identifies LEDs with different blink frequencies. Although it does not transmit binary information, and hence has limited communication capabilities, it can be utilized to track distinctive LEDs with light-weight algorithms for localization of robots [7, 25]. The interval-based protocol encodes information as the interval of two consecutive ON or OFF of LEDs. It can be used to localize the LED markers from a stationary event camera [4, 5, 28], as well as pan-tilt-angle estimation of a moving camera [22]. Recently the

change-based protocol has been proposed, which encodes information by changing the intensity of LEDs (i.e., modulation) [16, 35, 41].

3. Dataset

This section presents the details of the proposed dataset: hardware (camera and LED markers) settings (Sec. 3.1), recording scenarios (Sec. 3.2), and annotations (Sec. 3.3).

3.1. Hardware

Receiver. The E-VLC dataset focuses on the scenes where the receiver (cameras) moves at a walking speed, while the scene (including LED markers) is static. To this end, we build a custom mobile recording system equipped with two high-resolution cameras, a tablet, and a trigger box, enabling us to achieve high-quality calibration and synchronization. Although some cameras (e.g., DAVIS [2, 36]) can record co-located events and frames, their data quality and pixel pitch are insufficient for precise localization purposes. Our custom-built system consists of a high-resolution event camera (Prophesee IMX636, 1280×720 pix [8]) and a frame camera (Basler acA1300-200um, 1280×1024 pix). Both cameras have a slight baseline (i.e., stereo settings) and are recorded to a tablet (Surface 11 Pro, Ubuntu 22.02) via USB cables (see Fig. 2). The cameras are calibrated following [21]. Notice that there are small offsets between the cameras and the markers of the motion capture, which are inevitable by design. Event cameras are known to drop data or produce invalid timestamps when there is too much data (e.g., fast motion, flickering source), hence we choose the camera sensitivity carefully, as we report in Sec. 3.2.

The trigger box sends synchronization pulses at 120Hz to three different destinations: the two cameras and an ex-

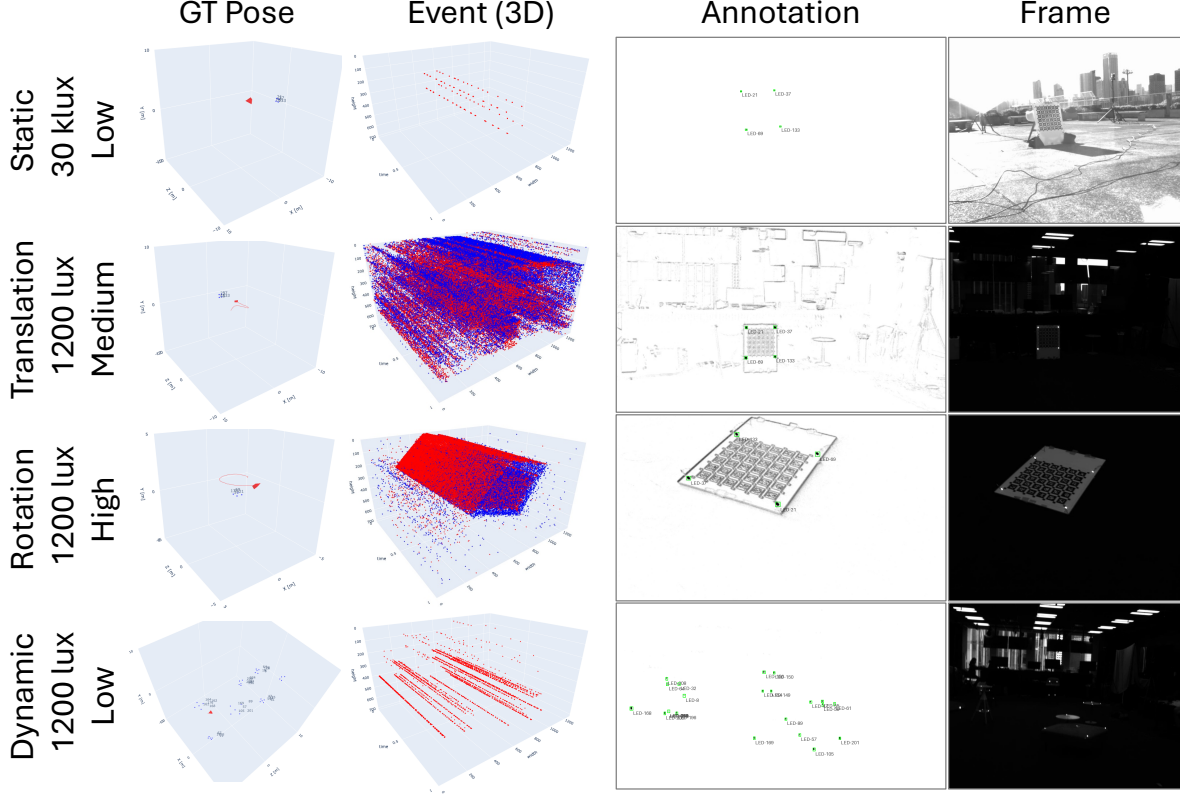


Figure 4. *Examples of the dataset.* Each row describes examples of different motion patterns, scene luminances, and camera sensitivities. The “Low” sensitivity sequences (first and last rows) only record markers, while others record markers and edges. Best viewed online (enlarged).

ternal motion capture (OptiTrack). We design one of the trigger cables to be 10 m so that it allows the recording device to move inside the motion capture system, which provides GT positions of the camera and LED markers at sub-millimeter accuracy at 100Hz. The recording sites are indoor and outdoor of about $15\text{m} \times 10\text{m}$ sizes. The frames are hardware-triggered and record videos at 40 fps. Figure 2 shows the recording system, scenes, and example data.

Transmitter. As LED markers, we use bullet-shaped LEDs (OSPG5111A, Green, 0.1 W) with a custom micro-controller that controls the LED modulation. One micro-controller controls five LEDs with different blink patterns, whose timings (temporal resolution) are synchronized. The data transmitted are a few bytes of numbers (IDs), and each LED repeats the assigned blink pattern, which is typically around 10 ms.

Several prior work have proposed modulation protocols (see Sec. 2). Among them, we choose the interval-based protocol, since (i) it is robust among others tested, (ii) it is popularly used (e.g., supported by Prophesee’s Metavision SDK [26] as well as other prior work [4, 5, 22, 28]), and (iii) it is robust against the tail-event effect of negative events in dark scenes, since it relies on positive (ON) events

only. The time-interval protocol parameters consist of the fundamental frequency f_b , the binary patterns, and the start pattern. In this work, we set $f_b = 5$ kHz, binary “0” as $1/f_b$, “1” as $2/f_b$, and start as $3/f_b$ that are distinguished with $1/f_b$ lighting off.

In total, we use 40 LED markers (i.e., 8 microcontrollers), all of which transmit different IDs. The markers are attached to different objects, such as boxes and tables, as well as an Aruco marker (printed on A1 size) to benchmark with frame-based localization methods. Figure 3 shows examples of LED markers and objects. The precise LED positions are measured with the motion capture system before the camera recordings.

3.2. Scenarios

The details of the sequences, conditions, and data statistics are summarized in Tab. 2. In total, the dataset consists of 110 sequences that include 7.5G events, 88k frames, and 266k annotations.

Motion type. We prepare four different camera motions: *static*, *translation*, *rotation*, and *dynamic*. All motions except for *static* are at a normal walking speed with the hand-held recorder. Figure 4 shows examples of the data.

Table 3. Event camera sensitivity settings.

	Bias (OFF)	Bias (ON)	High-pass filter
Low	180	60	120
Medium	70	60	60
High	45	45	30

Static sequences use four markers that are attached to the corner of the AprilGrid (see Fig. 3 (left) for the markers). During the recording, the device is mounted on a tripod and does not move. We test different locations with different distances and angles from the marker against a wall, spanning from 2 m to 14 m. *Translation* sequences use the same four LEDs and the Aruco marker, however, the recording device moves with mainly translational motion. Some sequences focus on the translation along the camera’s optic axis (i.e., perpendicular to the markers), to cover practical cases for mobile applications, while others include the translation along the other directions (i.e., parallel to the markers). In *rotation* sequences, the same markers are located on the floor, and the camera motion is mainly rotation, focusing on the marker in the field of view. Contrary to the other three patterns that use four LEDs, *dynamic* sequences use 35 LED markers that are attached to different objects, such as boxes and tables as shown in Fig. 3. The recording device moves freely among the objects and receives signals from partially visible LEDs.

Camera sensitivity. Since the LED markers emit high-frequency intensity changes, one could configure the event camera parameters (e.g., biases, high-pass filters) so that it only records such signals, discarding low-frequency events generated by moving edges in the scene. However, in practical use-cases of event cameras for VLC, it is important for the camera to receive both events from such moving edges and LEDs, so that the event data can be utilized in other computer vision tasks, such as motion estimation, object detection, and deblur. However, since LEDs generate lots of events and the cameras cannot guarantee proper timestamps beyond a certain amount of data (typically tens to hundreds of Mega-events per second), we carefully select three different parameters to record valid data. Table 3 describes the parameters tested: the *low* sensitivity is tuned best for the LED signals and rarely receives other events, the *high* sensitivity captures both LEDs and scene edges, and the *medium* sensitivity is in the middle of the two.

Scene luminance. We also provide sequences in various scene luminances to leverage the high-dynamic range of event cameras. The data is recorded both outside (on a sunny day) and inside, where we can control the luminance. The luminance conditions are among 10, 600, 1200, and 30k (bright outside), depending on sequences (see Tab. 2).

3.3. Annotations

After recording, we annotate bounding boxes of LED pixels with the IDs for the event camera data as shown in Fig. 4 (the third column). The annotation frames are based on the trigger signals (i.e., 120Hz). The LED light may cause glare in the event camera, especially when the camera is close enough to the light source, in which case the observed events form sharp tails from the center of the LED. We include such tails in the bounding boxes.

4. Methodology

In this section, we briefly summarize the LED detection and pose estimation from events in Sec. 4.1 and propose the motion compensation pipeline in Sec. 4.2.

4.1. LED detection and pose estimation

An event camera captures intensity changes at each pixel and generates a stream of events $e_k \doteq (\mathbf{x}_k, t_k, p_k)$, where (\mathbf{x}_k, t_k) is space-time coordinates and polarity $p_k \in \{+1, -1\}$ is the sign of the change. An event is generated when the logarithmic intensity L at a pixel \mathbf{x} changes by a certain threshold value C , i.e., $\Delta L(\mathbf{x}_k, t_k) \doteq L(\mathbf{x}_k, t_k) - L(\mathbf{x}_k, t_k - \Delta t_k) = p_k C$.

Although the intensity change due to the marker may be much larger than C , and hence an LED change (e.g., OFF to ON) may generate more than one event, we simply ignore such cases and focus on the time interval of events that are close enough to the base frequency of the LED blink. To this end, we use the time-map representation [6, 19] that stores the timestamp of a previous event at the same pixel \mathbf{x} . The time map $\mathcal{T}(\mathbf{x}_k) = t_k$ is updated using the timestamp of the new event t_{k+1} , if the time interval is larger than the previous time-map at the pixel \mathbf{x}_{t+1} with a tolerance τ ,

$$\mathcal{T}(\mathbf{x}_{k+1}) = t_{k+1}, \text{ if } t_{k+1} > \mathcal{T}(\mathbf{x}_{k+1}) + \frac{1}{f_b} - \tau. \quad (1)$$

The time-map provides the history of the time intervals of previous events, and we decode the marker IDs based on the series of the previous time-map since the start signal. After detecting and decoding LEDs, we use SQPNP [37] to estimate the camera pose, using the calibration parameters. Since our setting relies on the small number of keypoints (typically less than 10 pixels), we find that RANSAC does not contribute to stabilizing the pose estimation and hence we do not use it.

4.2. Motion Estimation and Compensation

Since the event camera moves, we observe that the detection accuracy degrades along with the displacement of the LED pixels in the image plane. One might use tracker algorithms, however, this requires integration with the time map representation, which we leave as future work. In this work,

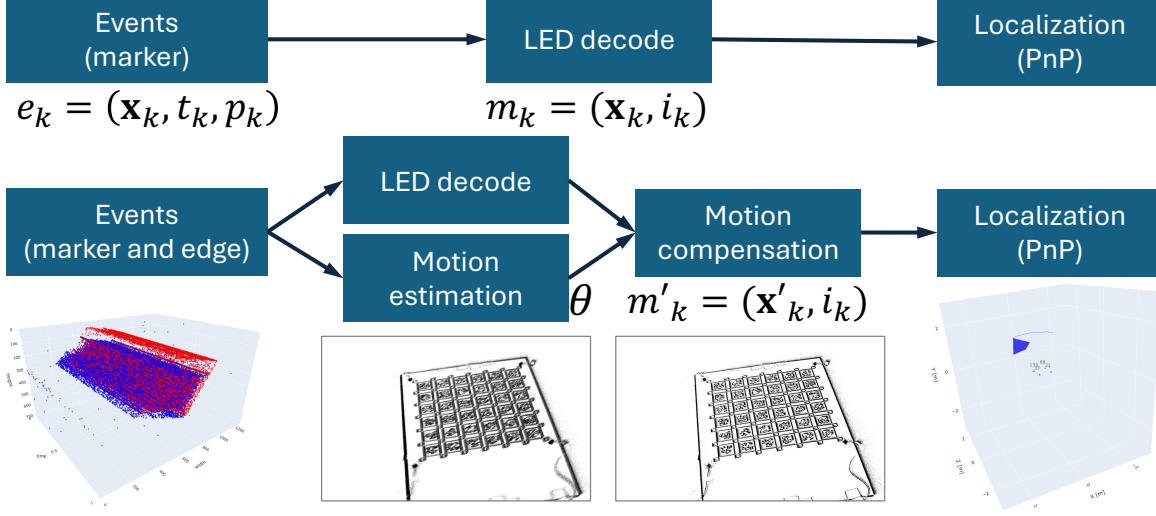


Figure 5. *Proposed motion compensation pipeline.* With the low camera sensitivity (the top diagram), LED information is decoded directly from events. With the middle or high sensitivities (bottom diagram), we leverage the motion estimation and compensation algorithms to improve the localization accuracy.

we propose to utilize motion estimation and compensation to improve the decoding and localization accuracy.

Contrast Maximization (CMax) [11] is a state-of-the-art method to estimate various motion from events alone, such as rotation [9, 14, 15, 17, 29], feature flow [27, 31, 34, 42, 43], and dense optical flow [30, 32]. In CMax, events $\mathcal{E} \doteq \{e_k\}_{k=1}^{N_e}$ are assumed being caused by moving edges (i.e., brightness constancy assumption), and are geometrically warped to $\mathcal{E}'_{t_{\text{ref}}} \doteq \{e'_k\}_{k=1}^{N_e}$ at a reference time t_{ref} using a motion model \mathbf{W} :

$$e_k \doteq (\mathbf{x}_k, t_k, p_k) \mapsto e'_k \doteq (\mathbf{x}'_k, t_{\text{ref}}, p_k). \quad (2)$$

Then, the warped events are aggregated on an image of warped events (IWE):

$$I(\mathbf{x}; \mathcal{E}'_{t_{\text{ref}}}, \theta) \doteq \sum_{k=1}^{N_e} \delta(\mathbf{x} - \mathbf{x}'_k), \quad (3)$$

as the histogram of the warped events \mathbf{x}'_k . The Dirac delta is approximated by a Gaussian, $\delta(\mathbf{x} - \boldsymbol{\mu}) \approx \mathcal{N}(\mathbf{x}; \boldsymbol{\mu}, \epsilon^2 \text{Id})$ with $\epsilon = 1$ pixel. Next, an objective function, such as the image contrast of the IWE (3) (e.g., [12]) measures the goodness of fit between the events and the warp parameter. As the warp models in this work, we use two types: feature flow $\mathbf{x}' = \mathbf{x} + (t - t_{\text{ref}})\boldsymbol{\theta}$ with a constant image velocity $\boldsymbol{\theta} \equiv (v_x, v_y)^\top$ for translational motion, and $\mathbf{x}^{h'} \sim \mathbf{R}(t\boldsymbol{\omega})\mathbf{x}^h$ with an angular velocity $\boldsymbol{\theta} \equiv (\omega_x, \omega_y, \omega_z)^\top$, calibrated homogeneous coordinates \mathbf{x}^h , and exponential coordinates $\mathbf{R}(\phi) \doteq \exp(\phi^\wedge)$ [1, 10] for rotational motion.

Our proposed pipeline is summarized in Fig. 5. Thanks to the parameter settings, we utilize the event information from scene edges (non-LEDs) to estimate the camera motion. After the motion estimation, we warp the events and

align its spatial coordinates, which we feed to the downstream LED detection and localization pipeline (Sec. 4.1). Furthermore, despite the brightness constancy assumption of the CMax framework, we find that CMax works well to estimate motion on low-sensitivity event data (i.e., events mainly from LED markers), which breaks the assumption.

5. Experiments

Metrics and baseline. For future benchmarking purposes, we provide the baseline results of the marker detection and localization. The metrics used to assess the LED decoding are detection rate (DR), which is the ratio of bounding boxes that have at least one pixel with the correct marker ID decoding. For the pose metrics, we report the L_1 error of the location. We compare the results between the proposed motion compensation (“Ours”) and without it (“Baseline”).

Hyper-parameters. The motion estimation is based on the Newton-CG optimization algorithm with a maximum of 50 iterations. The evaluation is at the frame timings (i.e., 40fps). We use the 3-DOF rotational motion for the rotation sequences and the 2-DOF feature flow for others.

Event-rate analysis. Event cameras need careful bias configurations when the scene includes flickering light sources due to possibly large amounts of data, as mentioned in Sec. 3.2. Here, we first provide further detailed analysis both for the simplest sequences (i.e., *static*) and the complex sequences (i.e., *dynamic*). Figure 6 shows the event rate in the unit of Mev/s (Mega-event per second) for the static and dynamic sequences. The static sequences do not expect events from the camera motion, regardless of the

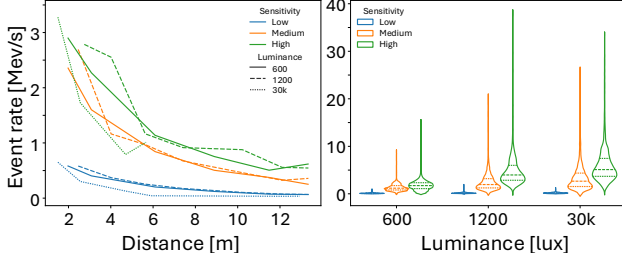


Figure 6. Event rate analysis. (left) The *static* sequences mainly consist of events from the LED markers. (right) The *dynamic* sequences consist of events from the LED markers and the camera motion, depending on the camera sensitivity.

Table 4. Comparison between frame-based localization and event-based localization using rotation sequences.

	Detected frames \uparrow	Mean [m] \downarrow	Median [m] \downarrow
Event (H)	4185	0.184	0.181
Frame	1038	0.171	0.178
Event (M)	3236	0.196	0.191
Frame	755	0.172	0.177
Event (L)	2871	0.204	0.197
Frame	374	0.171	0.173

sensitivity. The camera responds to the four LED markers, whose sizes in the image plane increase at closer distances. The dynamic sequences generate events from the markers and the camera motion, depending on the sensitivity. In all scene luminance conditions, the *high* sensitivity results in the largest amount of events, and we observe the camera drops data for even higher sensitivity (e.g., lower contrast threshold) or faster camera motion.

5.1. Comparison Between Events And Frames

Effective distance of localization. Figure 7 shows the effective distances of camera localization, comparing the LED-based (event-based) and the Aruco-based (frame-based) methods. The frame-based method can not detect the marker or localize in dark scenes (e.g., 600 lux). The effective distance for frames becomes shorter under 1200 lux than under 30k lux, however, the effective distance for events does not change significantly due to the scene brightness, clearly showcasing the advantage of LED-based localization.

Localization accuracy. Table 4 reports the comparison between frame-based and event-based localization on the *rotation* sequences (1200 lux), where the marker size is 0.5 m and the radius of the motion is roughly 2–3m. The accuracies between events (LED markers) and frames (Aruco markers) are similar, confirming the effectiveness of the LED-based localization. We observe slight (1–3 cm) perfor-

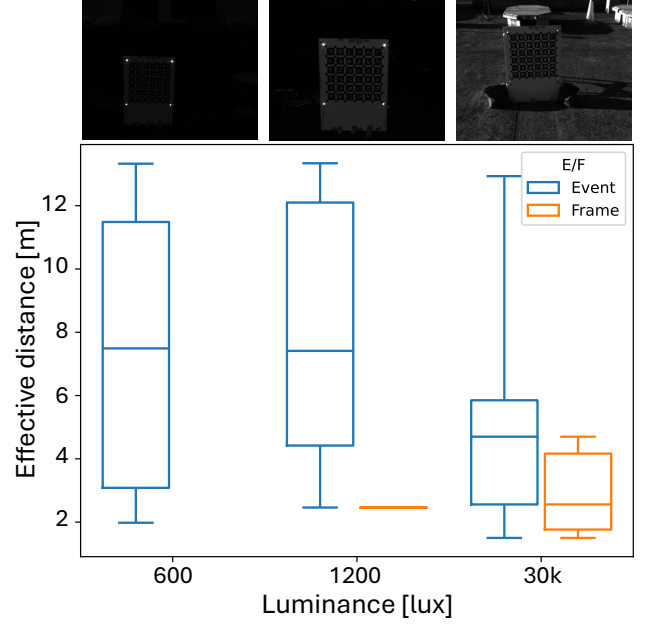


Figure 7. Effective marker detection distances for frames and events. Frame data collapse as the scene becomes darker, limiting the detection range, while event data do not suffer.

mance improvement with frames, which can be attributed by the number of markers used (36 markers, compared with 4 LEDs). Notice that LED detection is by far more successful than Aruco marker detection (i.e., “Detected frames”), which is due to motion blur in the frames. In conclusion, both results in Fig. 7 and Tab. 4 evidence that the LED-based localization works at larger distance and under various scene illumination, while maintaining the accuracy that is expected in the conventional frame-based method.

5.2. Results of LED Detection and Localization

The qualitative results for various sequences are shown in Fig. 8 for detection and in Fig. 9 for localization, respectively. We confirm that LEDs are successfully detected and decoded in most of the sequences. Table 5 reports the quantitative results of the detection rate, showing it achieves over 90% for all sequences. The detection fails under large pixel displacements, i.e., large motion of the camera.

The localization accuracy is also reported in Tab. 5. Our proposed motion compensation pipeline constantly achieves smaller errors than the baseline. Notice that the translation sequences consist of various distances (2–15 m) between the camera and the markers, which explains the relatively larger error (about 80 cm) compared with the rotation sequences (about 20 cm). The qualitative results (Fig. 9) show examples of the different errors based on the distance from the marker. We observe no significant differences in the pose errors among different camera sensitivities or scene illuminations.

Table 5. Results of LED detection and localization.

Sensitivity	Luminance	High				Medium				Low			
		1200		600		1200		600		1200		600	
		DR \uparrow	Pose [m] \downarrow	DR \uparrow	Pose [m] \downarrow	DR \uparrow	Pose [m] \downarrow	DR \uparrow	Pose [m] \downarrow	DR \uparrow	Pose [m] \downarrow	DR \uparrow	Pose [m] \downarrow
Translation(Z)	Baseline	0.908	1.105	0.966	1.093	0.903	1.168	0.965	1.234	0.977	0.934	0.991	1.036
	Ours	0.913	0.785	0.969	0.782	0.915	0.753	0.970	0.858	0.977	0.699	0.991	0.807
Translation(XYZ)	Baseline	—	—	—	—	0.978	0.834	0.950	0.795	0.967	0.852	0.969	0.673
	Ours	—	—	—	—	0.981	0.736	0.952	0.659	0.967	0.659	0.970	0.562
Rotation	Baseline	0.924	0.287	0.983	0.240	0.973	0.219	0.978	0.254	0.988	0.227	0.987	0.250
	Ours	0.929	0.247	0.983	0.189	0.975	0.177	0.980	0.206	0.989	0.175	0.988	0.211

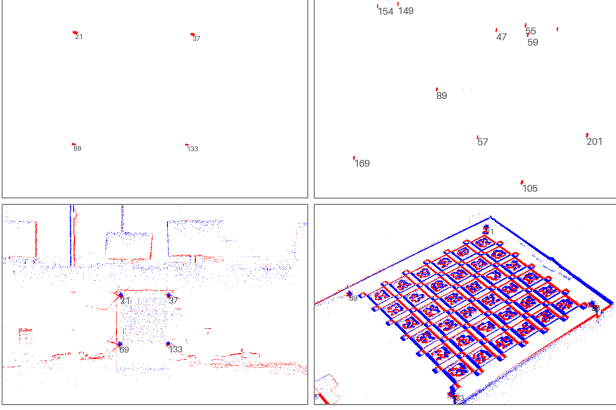


Figure 8. Detection results for different sequences. (Top) Low sensitivity, (Bottom) medium and high sensitivity.

6. Limitations

While we find that other light sources (i.e., other flickering light sources than LED markers) are not a problem due to the marker’s specific blink patterns, reflective surfaces in the scene may interfere the detection and localization. In practical applications, a more robust algorithm for localization is desirable, e.g., utilizing RANSAC.

The blink protocol does not have error corrections such as parity bits, hence it is important to explore a more robust protocol. We observe the latency of negative events increases under low illuminations (i.e., “tail” effect). This is reported to be specific to the sensor used (IMX636), hence different cameras could improve the error rate in the future.

In this work, we use simple motion models, such as feature flow and rotational motion, which the recording scenarios do not always fit. It would be desirable to combine SLAM (simultaneous localization and mapping) with the LED marker settings. Also, the proposed motion estimation and compensation increase the computation, hence it is important to benchmark the runtime.

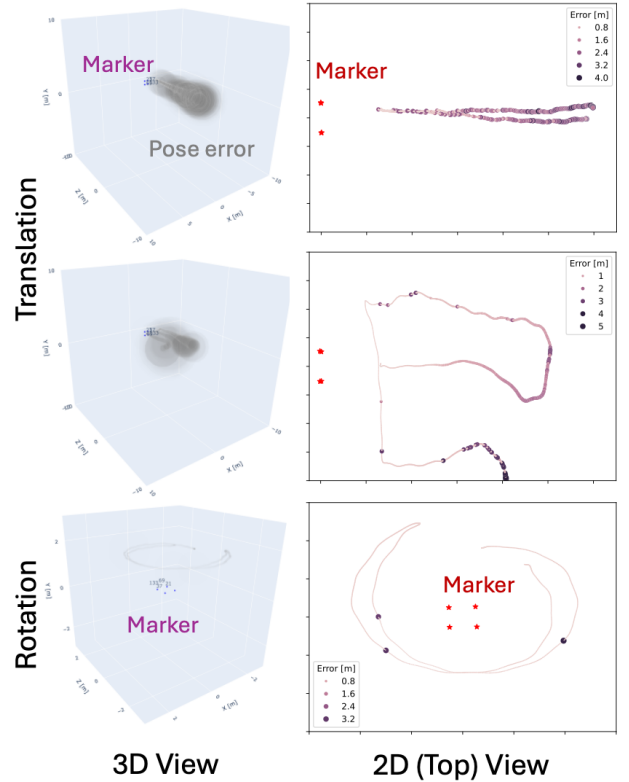


Figure 9. Results of localization errors.

7. Conclusion

This work presents the first public dataset (E-VLC) using modulated LEDs for event cameras, which consists of precisely synchronized events, frames, ground-truth pose of LED markers and cameras, and bounding-box annotations for LEDs in various recording conditions (motion type, scene luminance, event camera sensitivity) to cover real-world applications. We also propose a novel method using motion compensation based on Contrast Maximization that improves localization. We hope that the proposed dataset serves as a future benchmark for both motion-related classical computer vision tasks and LED marker decoding tasks simultaneously, broadening event camera applications.

References

- [1] T. D. Barfoot. *State Estimation for Robotics - A Matrix Lie Group Approach*. Cambridge University Press, 2015.
- [2] Christian Brandli, Raphael Berner, Minhao Yang, Shih-Chii Liu, and Tobi Delbruck. A 240x180 130dB 3 μ s latency global shutter spatiotemporal vision sensor. *IEEE J. Solid-State Circuits*, 49(10):2333–2341, 2014.
- [3] Alin-Mihai Căilean, Cătălin Beguni, Sebastian-Andrei Avătămăniței, and Mihai Dimian. Experimental demonstration of a 185 meters vehicular visible light communications link. In *IEEE Photonics Conference (IPC)*, pages 1–2. IEEE, 2021.
- [4] Andrea Censi, Jonas Strubel, Christian Brandli, Tobi Delbruck, and Davide Scaramuzza. Low-latency localization by active led markers tracking using a dynamic vision sensor. In *IEEE/RSJ International Conference on Intelligent Robots and Systems*, pages 891–898. IEEE, 2013.
- [5] Guang Chen, Wenkai Chen, Qianyi Yang, Zhongcong Xu, Longyu Yang, Jörg Conradt, and Alois Knoll. A novel visible light positioning system with event-based neuromorphic vision sensor. *IEEE Sensors Journal*, 20(17):10211–10219, 2020.
- [6] Tobi Delbruck. Frame-free dynamic digital vision. In *Proc. Int. Symp. Secure-Life Electron.*, pages 21–26, 2008.
- [7] Gerald Ebmer, Adam Loch, Minh Nhat Vu, Roberto Mecca, Germain Haessig, Christian Hartl-Nesic, Markus Vincze, and Andreas Kugi. Real-time 6-dof pose estimation by an event-based camera using active led markers. In *Proceedings of the IEEE/CVF Winter Conference on Applications of Computer Vision*, pages 8137–8146, 2024.
- [8] Thomas Finateu, Atsumi Niwa, Daniel Matolin, Koya Tsuchimoto, Andrea Mascheroni, Etienne Reynaud, Poooria Mostafalu, Frederick Brady, Ludovic Chotard, Florian LeGoff, Hirotsugu Takahashi, Hayato Wakabayashi, Yusuke Oike, and Christoph Posch. A 1280x720 back-illuminated stacked temporal contrast event-based vision sensor with 4.86 μ m pixels, 1.066Geps readout, programmable event-rate controller and compressive data-formatting pipeline. In *IEEE Int. Solid-State Circuits Conf. (ISSCC)*, pages 112–114, 2020.
- [9] Guillermo Gallego and Davide Scaramuzza. Accurate angular velocity estimation with an event camera. *IEEE Robot. Autom. Lett.*, 2(2):632–639, 2017.
- [10] Guillermo Gallego and Anthony Yezzi. A compact formula for the derivative of a 3-D rotation in exponential coordinates. *J. Math. Imaging Vis.*, 51(3):378–384, 2014.
- [11] Guillermo Gallego, Henri Rebecq, and Davide Scaramuzza. A unifying contrast maximization framework for event cameras, with applications to motion, depth, and optical flow estimation. In *IEEE Conf. Comput. Vis. Pattern Recog. (CVPR)*, pages 3867–3876, 2018.
- [12] Guillermo Gallego, Mathias Gehrig, and Davide Scaramuzza. Focus is all you need: Loss functions for event-based vision. In *IEEE Conf. Comput. Vis. Pattern Recog. (CVPR)*, pages 12272–12281, 2019.
- [13] Guillermo Gallego, Tobi Delbruck, Garrick Orchard, Chiara Bartolozzi, Brian Taba, Andrea Censi, Stefan Leutenegger, Andrew Davison, Jörg Conradt, Kostas Daniilidis, and Davide Scaramuzza. Event-based vision: A survey. *IEEE Trans. Pattern Anal. Mach. Intell.*, 44(1):154–180, 2022.
- [14] Cheng Gu, Erik Learned-Miller, Daniel Sheldon, Guillermo Gallego, and Pia Bideau. The spatio-temporal Poisson point process: A simple model for the alignment of event camera data. In *Int. Conf. Comput. Vis. (ICCV)*, pages 13495–13504, 2021.
- [15] Shuang Guo and Guillermo Gallego. CMax-SLAM: Event-based rotational-motion bundle adjustment and SLAM system using contrast maximization. *IEEE Trans. Robot.*, 40:2442–2461, 2024.
- [16] Damien Joubert, Mathieu Hébert, Hubert Konik, and Christophe Lavergne. Characterization setup for event-based imagers applied to modulated light signal detection. *Applied optics*, 58(6):1305–1317, 2019.
- [17] Haram Kim and H. Jin Kim. Real-time rotational motion estimation with contrast maximization over globally aligned events. *IEEE Robot. Autom. Lett.*, 6(3):6016–6023, 2021.
- [18] Takuya Kitade, Wataru Yamada, Keiichi Ochiai, and Michita Imai. Bicode: A hybrid blinking marker system for event cameras. In *2024 IEEE International Conference on Robotics and Automation (ICRA)*, pages 2939–2945. IEEE, 2024.
- [19] Xavier Lagorce, Garrick Orchard, Francesco Gallupi, Bertram E. Shi, and Ryad Benosman. HOTS: A hierarchy of event-based time-surfaces for pattern recognition. *IEEE Trans. Pattern Anal. Mach. Intell.*, 39(7):1346–1359, 2017.
- [20] Patrick Lichtsteiner, Christoph Posch, and Tobi Delbruck. A 128x128 120dB 30mW asynchronous vision sensor that responds to relative intensity change. In *IEEE Int. Solid-State Circuits Conf. (ISSCC)*, pages 2060–2069, 2006.
- [21] Manasi Muglikar, Mathias Gehrig, Daniel Gehrig, and Davide Scaramuzza. How to calibrate your event camera. In *IEEE Conf. Comput. Vis. Pattern Recog. Workshops (CVPRW)*, pages 1403–1409, 2021.
- [22] Georg R Müller and Jörg Conradt. A miniature low-power sensor system for real time 2d visual tracking of led markers. In *IEEE International Conference on Robotics and Biomimetics*, pages 2429–2434. IEEE, 2011.
- [23] Michael Plattner and Gerald Ostermayer. Camera-based vehicle-to-vehicle visible light communication-a software-only solution for vehicle manufacturers. In *32nd International Conference on Computer Communications and Networks (ICCCN)*, pages 1–7. IEEE, 2023.
- [24] Christoph Posch, Daniel Matolin, and Rainer Wohlgenannt. An asynchronous time-based image sensor. In *IEEE Int. Symp. Circuits Syst. (ISCAS)*, pages 2130–2133, 2008.
- [25] Mohammed Salah, Mohammed Chehadah, Muhammad Humais, Mohammed Wahbah, Abdulla Ayyad, Rana Azzam, Lakmal Seneviratne, and Yahya Zweiri. A neuromorphic vision-based measurement for robust relative localization in future space exploration missions. *IEEE Trans. Instrum. Meas.*, 73:1–12, 2022.
- [26] Metavision SDK. *Modulated Light Detection* [Online]. Available: https://docs.prophesee.ai/stable/samples/modules/cv/active_marker_2d_tracking_cpp.html, 2025. [Accessed: 10 March 2025].

- [27] Hochang Seok and Jongwoo Lim. Robust feature tracking in dvs event stream using Bezier mapping. In *IEEE Winter Conf. Appl. Comput. Vis. (WACV)*, pages 1647–1656, 2020.
- [28] Wen-Hsuan Shen, Po-Wen Chen, and Hsin-Mu Tsai. Vehicular visible light communication with dynamic vision sensor: A preliminary study. In *IEEE Vehicular Networking Conference (VNC)*, pages 1–8. IEEE, 2018.
- [29] Shintaro Shiba, Yoshimitsu Aoki, and Guillermo Gallego. A fast geometric regularizer to mitigate event collapse in the contrast maximization framework. *Adv. Intell. Syst.*, page 2200251, 2022.
- [30] Shintaro Shiba, Yoshimitsu Aoki, and Guillermo Gallego. Secrets of event-based optical flow. In *Eur. Conf. Comput. Vis. (ECCV)*, pages 628–645, 2022.
- [31] Shintaro Shiba, Yoshimitsu Aoki, and Guillermo Gallego. Event collapse in contrast maximization frameworks. *Sensors*, 22(14):1–20, 2022.
- [32] Shintaro Shiba, Yannick Klose, Yoshimitsu Aoki, and Guillermo Gallego. Secrets of event-based optical flow, depth, and ego-motion by contrast maximization. *IEEE Trans. Pattern Anal. Mach. Intell.*, 46(12):7742–7759, 2024.
- [33] Shintaro Shiba, Quan Kong, and Norimasa Kobori. Augmented reality applications using active markers with an event camera. In *IEEE Conf. Comput. Vis. Pattern Recog. Workshops (CVPRW)*, 2025.
- [34] Timo Stoffregen and Lindsay Kleeman. Event cameras, contrast maximization and reward functions: an analysis. In *IEEE Conf. Comput. Vis. Pattern Recog. (CVPR)*, pages 12292–12300, 2019.
- [35] Zhengqiang Tang, Takaya Yamazato, and Shintaro Arai. A preliminary investigation for event camera-based visible light communication using the propeller-type rotary led transmitter. In *2022 IEEE International Conference on Communications Workshops (ICC Workshops)*, pages 646–650. IEEE, 2022.
- [36] Gemma Taverni, Diederik Paul Moeys, Chenghan Li, Celso Cavaco, Vasyl Motsnyi, David San Segundo Bello, and Tobi Delbruck. Front and back illuminated Dynamic and Active Pixel Vision Sensors comparison. *IEEE Trans. Circuits Syst. II (TCSII)*, 65(5):677–681, 2018.
- [37] George Terzakis and Manolis Lourakis. A consistently fast and globally optimal solution to the perspective-n-point problem. In *Eur. Conf. Comput. Vis. (ECCV)*, pages 478–494. Springer, 2020.
- [38] Ziwei Wang, Yonhon Ng, Jack Henderson, and Robert Mahony. Smart visual beacons with asynchronous optical communications using event cameras. In *IEEE/RSJ Int. Conf. Intell. Robot. Syst. (IROS)*, pages 3793–3799. IEEE, 2022.
- [39] Haswani Binti Che Wook, Shinichiro Haruyama, and Masao Nakagawa. Visible light communication with led traffic lights using 2-dimensional image sensor. *IEICE transactions on fundamentals of electronics, communications and computer sciences*, 89(3):654–659, 2006.
- [40] Takaya Yamazato, A Ohmura, Hiraku Okada, Toshiaki Fujii, Tomohiro Yendo, Shintaro Arai, and Koji Kamakura. Range estimation scheme for integrated i2v-vlc using a high-speed image sensor. In *IEEE International Conference on Communications Workshops (ICC)*, pages 326–330. IEEE, 2016.
- [41] Yue You, Mingzhu Zhu, Bingwei He, and Yihong Wang. Temporal feature markers for event cameras. *Journal of Real-Time Image Processing*, 21(2):41, 2024.
- [42] Alex Zihao Zhu, Nikolay Atanasov, and Kostas Daniilidis. Event-based visual inertial odometry. In *IEEE Conf. Comput. Vis. Pattern Recog. (CVPR)*, pages 5816–5824, 2017.
- [43] Alex Zihao Zhu, Nikolay Atanasov, and Kostas Daniilidis. Event-based feature tracking with probabilistic data association. In *IEEE Int. Conf. Robot. Autom. (ICRA)*, pages 4465–4470, 2017.